A rotation–extended cepstrum technique optimized by systematic analysis of various sets of X–ray images*

Thomas Lehmann[1], Carsten Goerke[1], Walter Schmitt[2], Ansgar Kaupp[3], Rudolf Repges[1]

[1]Institute of Medical Informatics and Biometry
[2]Clinic for Oral, Maxillofacial, and Facial Plastic Surgery
[3]Institute for Measurement Technology
The Aachen University of Technology (RWTH), D - 52057 Aachen, Germany
Email: lehmann@vaire.imib.rwth-aachen.de

ABSTRACT

Spatial registration is a major problem arising whenever several images of similar contents are to be compared. Considering translations only, two–dimensional cepstral techniques have been proven to be exact and robust against noise or intensity variations. Furthermore, the cepstral filtering is numerically more efficient than most common approaches to image registration based on cross–correlation or template matching.

In a previous paper,[1] we proposed a two–dimensional cepstrum based matching technique accessing rotations and translations. The logarithmic polar mapping of the power spectra of both images to be registered is used for the decoupling of rotations and translations (similar to the Fourier–Mellin transform). Rotations are detected first matching the mapped spectra by two–dimensional cepstrum analysis. After rotating back one image, the relative shift is determined using the same cepstrum technique. In clinical practise, the rotation detection step was discovered as the weakness of this registration technique.

Based on 855 pairs of dental radiographs acquired in known positions, three different approaches of matching the mapped spectra are compared: the cepstrum technique, the cross–correlation, and the entropy of the one–dimensional histogram distribution function of the subtraction image of the mapped spectra. The combination of the log–polar mapped power spectra of both X rays with the entropy–measure allows the best detection of rotations. The union with common cepstrum methods correcting translations results in a robust rotation–extended cepstrum technique.

Keywords: Medical X–Ray Imaging, Dental Radiology, Computer Assisted Diagnosis, Digital Image Processing, Pattern Recognition, Image Registration, Cepstrum Analysis, Fourier–Mellin Transform, Hartley Transform, RST–Invariant Image Descriptors

*This research is part of the project *Free–hand Subtraction Radiography*. The support of the German Research Community (DFG grant No. Re 427/5–1) is greatfully acknowledged.

0-8194-2085-9/96/$6.00

1 INTRODUCTION

Spatial registration of multispectral or multitemporal digital images is a major problem arising whenever data of a recording system have to be compared, and is therefore a focus of recent discussion in image processing.[2,3] To obtain a comparison on a pixel by pixel base, it is necessary to spatially register the images and correct the geometric distortions, e.g. translational and rotational movements, with sufficient accuracy. A matching algorithm should be robust with respect to noise and accurate even if the same pattern has different intensities and/or different positions and orientations in the two images to be registered. Furthermore, a matching algorithm should be numerically efficient.

The most common matching approach is based on the cross–correlation function and is also referred to as template matching.[4] It is derived assuming white noise distorting the object in the image. The size of the object determines the template's dimension. It corresponds directly to the computing time required for the calculation of all possible values of the parameters describing the geometric transform relating the object to its representation in the reference image. While such an extensive calculation is extremely time consuming, moments or moment invariants based matching techniques are used,[5] especially if further distortions can be expected. Those techniques are often applied to the binary representation of the object (e.g. character recognition) or the object's outlines.

In the field of medical image processing, the object/background model is invalid, i.e. the entire image is the object. In this case, several alternatives to the cross–correlation function have been proposed. In one group of matching techniques, the cross–correlation is exchanged by other correlation–like functions, e.g. the standard deviation of the difference image,[6,7] or the number of sign changes along the lines of the difference image.[8,9] Since all these techniques at least require the geometric transform of one image for all possible values of the parameters, those algorithms are numerically inefficient.

Another group of matching techniques bases on Fourier spectral or cepstral analysis. The two–dimensional cepstral techniques have been proven to be very accurate and characterized by an outstanding robustness against uncorrelated noise and intensity distortions.[10] In addition, cepstral filtering requires no segmentation of the images. However, the classical way of cepstrum analysis is restricted to the detection of translational shifts only and the pictures are not allowed to differ in rotation. Therefore, an extension to the detection of both, translation and rotation was proposed by the authors in a previous paper.[1]

In this paper, we describe the optimization of the rotation–extended cepstrum technique for its application in dental radiology. A total of 855 different pairs of in vitro acquired radiographs with a priori known misalignments were systematically analysed comparing the results of three approaches for the rotation detection step: cepstrum filter, cross–correlation, and entropy of the one–dimensional histogram function of the subtraction image.

The next section introduces the Fourier and the Mellin transforms and their combination to an invariant image descriptor. All three techniques use the decomposition of rotation and translation by this descriptor. Section 3 reviews the cepstrum technique and the three extensions to rotations. Computational aspects and efficient implementation using the Hartley transform are described in Section 4. Our method acquiring X–ray images with a priori known shifts and the results registering 855 pairs of dental radiographs are succeeding documented in Sections 5 and 6.

2 FOURIER–MELLIN INVARIANT IMAGE DESCRIPTORS

In this section the Fourier and Mellin transforms are introduced and combined to a rotation–, scaling–, and translation– (RST–) invariant image descriptor.

2.1 Fourier transform

The integral transforms[11]

$$F(\omega) = \int_{-\infty}^{\infty} f(t)e^{-j\omega t}dt \qquad \text{and} \qquad f(t) = \frac{1}{2\pi}\int_{-\infty}^{\infty} F(\omega)e^{j\omega t}d\omega \tag{1}$$

are well known as Fourier and inverse Fourier transform, respectively. One can easily show, that the magnitude of the two–dimensional Fourier transform $|F(u,v)|$ of the image function $f(x,y)$ is invariant to translations in the image plane, while rotations in the (x,y) plane are transformed to equal rotations in the (u,v) plane, and scaling is inverted,[11] e.g. expansions are transformed to shrinkings.

2.2 Mellin transform

The Mellin transform $M(s)$ of a continuous one–dimensional function $f(z)$ is given by[12,13]

$$M(s) = \int_0^{\infty} f(z)z^{s-1}dz \qquad \text{and} \qquad f(z) = \frac{1}{j2\pi}\int_{c-j\infty}^{c+j\infty} M(s)z^{-s}ds \tag{2}$$

denoting the inverse Mellin transform, respectively, where c is the real part of the complex variable $s = c + j\omega$. The Mellin transform is usually used to compute the moments of $f(z)$.[11] For example, area, first, and second moments of $f(z)$ are equal to $M(1)$, $M(2)$, and $M(3)$, respectively, and the second moment about centroid is $M(3) - [M(2)]^2/M(1)$.

Substituting z by e^{-t} we obtain $\ln(z) = -t$ and $dz/dt = -e^{-t}$. Furthermore, the integration limits in (2) transforms like $z \to 0 \Rightarrow t \to \infty$ and $z \to \infty \Rightarrow t \to -\infty$ and the Mellin transform becomes

$$M(s) = \int_{\infty}^{-\infty} f(e^{-t})e^{-t(s-1)}(-e^{-t})dt = \int_{-\infty}^{\infty} f(e^{-t})e^{-st}dt = L(s) \tag{3}$$

with $L(s)$ denoting the two–sided Laplace transform of a function with distorted coordinates $f'(t) = f(e^{-t})$. Further substituting $s = j\omega$ in (3) yields (1). Therefore, the undamped Mellin transform

$$M(\omega) = \int_0^{\infty} f(z)z^{-j\omega-1}dz = \int_{-\infty}^{\infty} f(e^{-t})e^{-j\omega t}dt \tag{4}$$

is computable by the Fourier transform (1), if the coordinate $t \to \ln(1/t)$ is logarithmically deformed at first

$$t \equiv e^{-(\ln(\frac{1}{t}))} \equiv e^{-(-\ln(t))} \tag{5}$$

Let f_1 and f_2 be two functions differing only in scale $f_2(z) = f_1(\alpha z)$, then the substitution: $\tau = \alpha z$, $z = \tau/\alpha$, $dz = d\tau/\alpha$ in (4) yields

$$M_2(\omega) = \int_0^{\infty} f_1(\alpha z)z^{-j\omega-1}dz = \int_0^{\infty} f_1(\tau)\tau^{-j\omega-1}(\frac{1}{\alpha})^{-j\omega-1}\frac{1}{\alpha}d\tau = \alpha^{j\omega}M_1(\omega) \tag{6}$$

One can easily recognize, that because of $|\alpha^{j\omega}| = |e^{j\omega\ln\alpha}| = 1$ equation (6) holds $|M_1(\omega)| = |M_2(\omega)|$. Therefore, the magnitude of a Mellin transformed function is invariant to scales.

2.3 RST–invariant image descriptors

An overview of invariant image descriptors is given elsewhere.[5] In the following, the Fourier and the Mellin transformations are combined to a RST–invariant image descriptor similar introduced by *Schalkoff*[14] or *Haken.*[15]

Therefore, let f_1 and f_2 be two given functions with f_2 being a (x_0, y_0) shifted, α rotated, and β scaled version of f_1

$$f_2(x,y) = f_1\Big(\beta(x\cos\alpha + y\sin\alpha) - x_0, \beta(-x\sin\alpha + y\cos\alpha) - y_0\Big) \tag{7}$$

The Fourier power spectra are computed to

$$|F_2(u,v)|^2 = \left|\frac{1}{\beta^2}F_1\left(\frac{u\cos\alpha + v\sin\alpha}{\beta}, \frac{-u\sin\alpha + v\cos\alpha}{\beta}\right)\right|^2 \tag{8}$$

This representation of the functions f depends only on the angle of rotation α and the amount of scale β. Both may be decoupled applying a transformation to polar coordinates (Fig. 1). Taking into account the addition theorems of trigonometric functions, the substitution $u = r\cos\varphi$ and $v = r\sin\varphi$ in (8) yields

$$|F_2(r\cos\varphi, r\sin\varphi)|^2 = \left|\frac{1}{\beta^2}F_1\left(\frac{r\cos(\varphi-\alpha)}{\beta}, \frac{r\sin(\varphi-\alpha)}{\beta}\right)\right|^2 \tag{9}$$

Denoting the power spectra in (9) as functions of (r, φ) leads to

$$|F_2(r,\varphi)|^2 = \left|\frac{1}{\beta^2}F_1\left(\frac{r}{\beta}, \varphi - \alpha\right)\right|^2 \tag{10}$$

Scalings are transformed into stretches of the r–axis, while rotations are mapped to shifts along the φ–axis. Applying the scale–invariant Mellin transform (4) to the r–coordinate and the shift–invariant Fourier transform

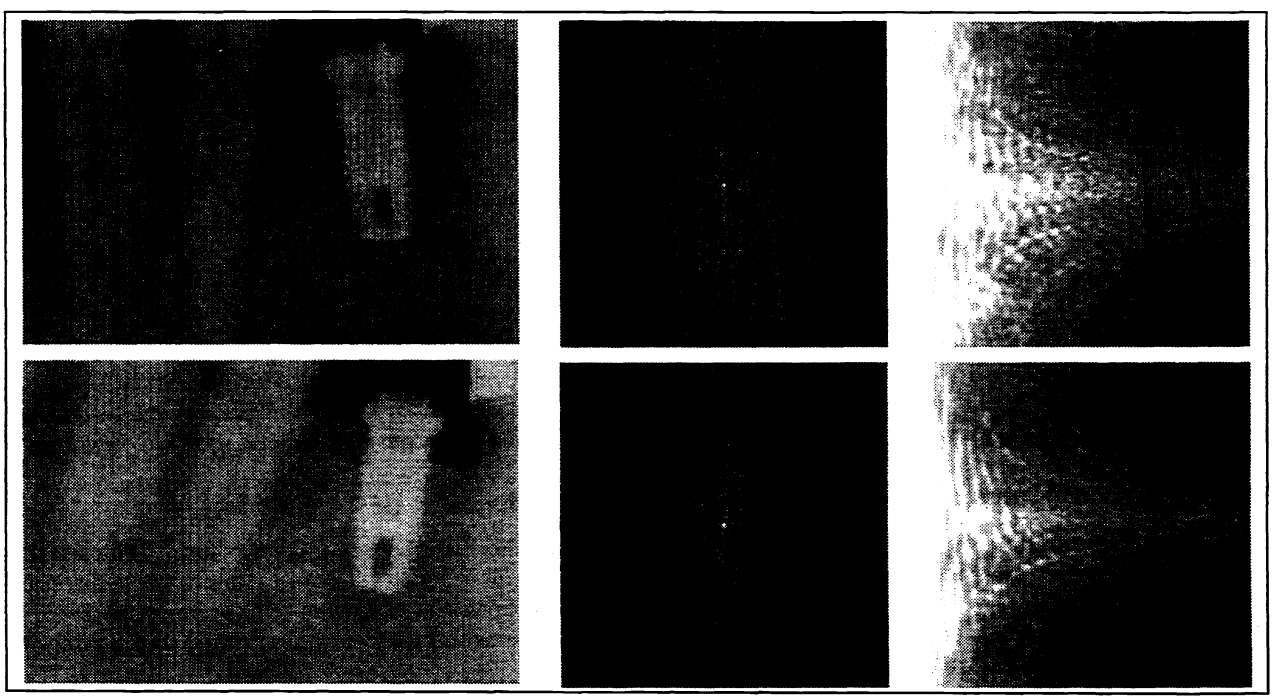

Figure 1: LOGARITHMIC POLAR MAPPING OF FOURIER POWER–SPECTRA
The images $f(x,y)$ on the left show dental X rays. Teeth as well as implants are figured. The Fourier power–spectra $|F(u,v)|$ are shown in the middle. Note their translation invariance while their rotational orientation corresponds to that in the spatial domain. The results of logarithmic polar mapping $|F(\rho,\varphi)|$ are displayed on the right in each line, respectively. Rotations are transformed into shifts along the vertical axis.

(1) to the φ–coordinate (Fourier–Mellin transform) equation (10) results in a RST–invariant image representation of both functions f_1 and f_2. As shown in Paragraph 2.2, the Mellin transform can be calculated using the Fourier transform if the coordinate $\rho = -\ln(r)$ is mapped logarithmically. Combining (5) and (10) yields

$$|F_2(\rho,\varphi)|^2 = \left|\frac{1}{\beta^2} F_1\Big(\rho + \ln(\beta), \varphi - \alpha\Big)\right|^2 \tag{11}$$

A further calculation of the Fourier power–spectra of the functions given in (11) results in a RST–invariant image descriptor

$$|M_2(u,v)|^2 \sim |M_1(u,v)|^2 \tag{12}$$

The mapping of multiplications (coordinate–scale) to additions (coordinate–shift) is a well known feature of the logarithm. Therefore, related methods are often used without referring to as Fourier–Mellin transform.[1,2,16]

3 THE CEPSTRUM TECHNIQUE

The next paragraph recapitulates the classical cepstrum technique for the detection of pure translational shifts. Based on the Fourier–Mellin RST–invariant image descriptors, different extensions to rotational shifts are proposed in the subsequent paragraphs.

3.1 Classical cepstrum

The cepstrum analysis was developed as an one–dimensional technique to examine seismographic data containing echos of some arbitrary wave packets.[17,18] In 1975 the (power–)cepstrum was derived again from the homomorphic system theory.[19] Based on the separability of the discrete Fourier transform (DFT) $\mathcal{F}\{\cdot\}$ cepstral filtering can easily be transferred to the two–dimensional image processing. In general, the power–cepstrum of a function f is the power–spectrum of the logarithm of the function's power–spectrum. Therefore, the two–dimensional power–cepstrum $\mathcal{C}\{\cdot\}$ may be defined in the spatial domain (x,y) as

$$\mathcal{C}\{f(x,y)\} = \left|\mathcal{F}\Big\{\log\left|\mathcal{F}\{f(x,y)\}\right|^2\Big\}\right|^2 \tag{13}$$

Using the most common way of cepstral filtering to estimate a scene's translational shift, first of all the two images to compare with are placed next to next in the center of a so called cepstrum window. Assume a cepstrum window consisting of the reference image $r(x,y)$ on the left hand side and the subsequent test image $t(x,y) = a_0 r(x-x_0, y-y_0)$ on the right hand side. Then, the resulting cepstrum window $g(x,y)$ may be expressed like

$$g(x,y) = r(x,y) + t(x-D,y) = r(x,y) \star \Big[\delta(x,y) + a_0\delta(x-(D+x_0), y-y_0)\Big] \tag{14}$$

where a_0 is an amplitude scale factor and D describes the dimension of the square images r and t. The relative translational shifts between both images are written in the spatial x–direction in terms of x_0 and in the y–direction in terms of y_0. A stepwise calculation of the power–cepstrum (13) shows the logarithm of the power–spectrum of the composite signal g containing cosinusoidal ripples whose amplitude and frequency are related to the intensity factor a_0 and the translatory displacements $D + x_0$ and y_0

$$G(u,v) = R(u,v)\cdot\Big(1 + a_0 e^{-i2\pi(u(D+x_0)+vy_0)}\Big) \tag{15}$$

$$\begin{aligned}\log|G(u,v)|^2 &= \log|R(u,v)|^2 + \log\Big(1 + 2a_0\cos\big(2\pi(u(D+x_0)+vy_0)\big) + a_0^2\Big)\\ &= \log|R(u,v)|^2 + \log|1+a_0^2| + \frac{2a_0}{1+a_0^2}\cos\big(2\pi(u(D+x_0)+vy_0)\big) \mp \ldots\end{aligned} \tag{16}$$

where $R(u,v)$ and $G(u,v)$ are the Fourier transforms in the frequency domain (u,v) of the reference image and the cepstrum window, respectively. In (16) the power series expansion $\log(1+x) = \sum_{n=1}^{\infty}(-1)^{n+1}x^n/n$ with $-1 < x \leq 1$ is inserted. A second power–spectrum operation is performed to obtain the power–cepstrum of $g(x,y)$

$$\mathcal{C}\{g(x,y)\} = \mathcal{C}\{r(x,y)\} + A\delta(x,y) + B\delta(x \pm (x_0+D), y \pm y_0) + C\delta(x \pm 2(x_0+D), y \pm 2y_0) + \ldots \qquad (17)$$

which equals the power–cepstrum of the reference image plus a train of delta functions occuring at integer multiplies of the translational shifts $(D+x_0, y_0)$. Thus, the translational difference between two images can simply be detected by inspecting the distance between the origin and the location of the first maximum peak in the cepstral plane.

Although this classical cepstrum technique requires no segmentation and is reliable, efficient, and immune to noise (Fig.2), it has the disadvantage of being sensitive to rotational changes between the images being registered.

3.2 Rotation–extended cepstrum Technique

An extension to rotations of classical cepstrum filtering can be given using the Fourier–Mellin RST–invariant image descriptor. The logarithmic polar mapping of the Fourier power–spectra (11) yields an image representation where translations are eliminated and rotations and scales are mapped into shifts. Those may be detected applying the classical cepstrum (17). After appropriately rotating and scaling one of the images, the cepstrum technique (17) may be applied again with $\alpha = 0$ and $\beta = 1$ in (7) now.[1]

3.3 Optimization for Dental Radiographs

In dental radiology, scales are neglectable. The X–ray tube is touching the patient's face and the intraoral film is pressed onto jaw and teeth. The approximation $\beta \approx 1$ in (11) leads to

$$|F_2(\rho,\varphi)|^2 = |F_1(\rho,\varphi-\alpha)|^2 \qquad (18)$$

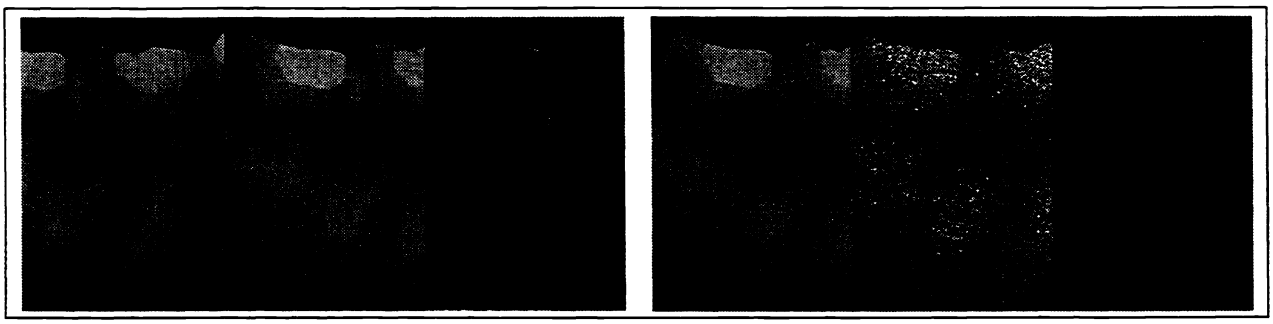

Figure 2: REGISTRATION OF TRANSLATIONS USING THE CLASSICAL CEPSTRUM TECHNIQUE
The figure's left part illustrates the classical cepstrum's property registering very large shifts (up to 50% of the width of images). The original–, the reference–, and the subtraction–image after registration are displayed adjacently from left to right. The dark bar in the difference image results from subtracting non–overlapping regions. The example on the right demonstrates the robustness of the technique with respect to noise (down to signal–to–noise ratios below 1.0).[10]

and therefore, the registration step for rotation detection has to be performed only in one dimension. Since cepstral techniques always assess two dimensions, correlation based methods can be easily designed to registrate only one dimension.

The cross–correlation function

$$\mathrm{CCF}(t) = \sum_{\rho}\sum_{\varphi}\left(\left|F_1(\rho,\varphi+t)\right|^2 \cdot \left|F_2(\rho,\varphi)\right|^2\right) \tag{19}$$

can be used efficiently, where the maximum $\mathrm{CCF}_{\max} = \mathrm{CCF}(\alpha)$ indicates the rotation angle α to be detected. Nevertheless, a lot of multiplications are required to compute the cross–correlation (19).

The amount of computation is drastically reduced, if the similarity measure is constructed from an one–dimensional function. Let $d_t(\rho,\varphi)$ be the subtraction of the functions F_1 and F_2 defined in (18) which can be calculated without any multiplications

$$d_t(\rho,\varphi) = \left|F_1(\rho,\varphi+t)\right|^2 - \left|F_2(\rho,\varphi)\right|^2 \tag{20}$$

and t again denoting the misalignment in the φ–axis. Then, the histogram distribution $h_t(p)$ provides an one–dimensional function describing the similarity between F_1 and F_2 depending on the parameter t, where p is in the range of values of d_t. The standard deviation[20] or the entropy[21,22] of the histogram of the difference image

$$\mathrm{EHDI}(t) = -1 \cdot \sum_{g} h_t(p) \cdot \log\big(h_t(p)\big) \tag{21}$$

may be used to evaluate the best adjustment with $\mathrm{EHDI}_{\max} = \mathrm{EHDI}(\alpha)$ indicating the rotational angle α to be detected.

4 IMPLEMENTATION

Some preprocessing steps are used to improve the results of cepstrum filtering. These methods are described next while the computational improvement applying the discrete Hartley transform is shown in the last paragraph of this section.

4.1 Preprocessing

The discrete Fourier transform (DFT) assumes the images to be periodic. To avoid artefacts resulting from the non–periodic property of finite images, windowing is required.[18] In our application, the Kaiser–Bessel window $w(n)$ for the dimension of the image $N, 0 \le n < N$ is approximated by[23]

$$w(n) = b_0 - b_1\cos\left(2\pi\frac{n}{N}\right) - b_2\cos\left(2\pi\frac{2n}{N}\right) - b_3\cos\left(2\pi\frac{3n}{N}\right) \quad \text{with} \quad \begin{cases} b_0 = 0.40243 \\ b_1 = 0.49804 \\ b_2 = 0.09831 \\ b_3 = 0.00122 \end{cases} \tag{22}$$

The algorithms for the fast Fourier transform (FFT) are usually limited to images with dimensions of powers of two. Zero–padding all images before transforming allows the handling of arbitrary dimensions of the image's column or row length. Additional preprocessing by sobel–filtering is also applied to emphasize edge–information.[10] In addition, the Fourier spectra are histogram optimized by stretching their logarithmic scale before they are mapped into polar coordinates. The resulting block diagram is presented in Figure 3.

The logarithmic polar mapping is used to turn rotations into translations along the φ–axis. In order to calculate the logarithmic polar mapping on discrete image data, the spatially variant resolution of the logarithmic domain has to be considered. The sampling rate decreases rapidly towards the image margins, so that an anti–aliasing filter must be provided.

4.2 Hartley transform

The discrete Hartley transform (DHT) may be used in cases where data is in the real domain and phase information is not required to substitute the more commonly used DFT designed for complex data. The benefits of calculating power–spectra and power–cepstra using the DHT are about 50% less required memory and about 40% faster program execution, at no loss in accuracy.[24]

The DHT was introduced as a sum of double–sided sine and cosine transforms,[25,26] basing on the continuous integral transform presented by *Hartley*[27] already in 1942. Let $H_s(u,v)$ be the separated DHT of an $M \times N$ image $f(x,y)$

$$H_s(u,v) = \sum_{x=0}^{M-1}\sum_{y=0}^{N-1} f(x,y)\,\mathrm{cas}(2\pi ux)\,\mathrm{cas}(2\pi vy) \quad \text{and} \quad f(x,y) = \frac{1}{MN}\sum_{u=0}^{M-1}\sum_{v=0}^{N-1} H_s(u,v)\,\mathrm{cas}(2\pi ux)\,\mathrm{cas}(2\pi vy) \tag{23}$$

denoting the inverse Hartley transform, respectively, with $\mathrm{cas}(\theta) = \cos(\theta) + \sin(\theta)$ being an abbreviation adopted from *Hartley*.[27] According to (23), the Fourier power–spectrum is calculated exploiting the relationship between the DHT and the power–spectrum[28]

$$|F(u,v)|^2 = \frac{1}{4}\left[H_s(-u,v) + H_s(u,-v)\right]^2 + \frac{1}{4}\left[H_s(u,v) - H_s(-u,-v)\right]^2 \tag{24}$$

Algorithms for fast Hartley transforms (FHT) are described elsewhere.[29,30]

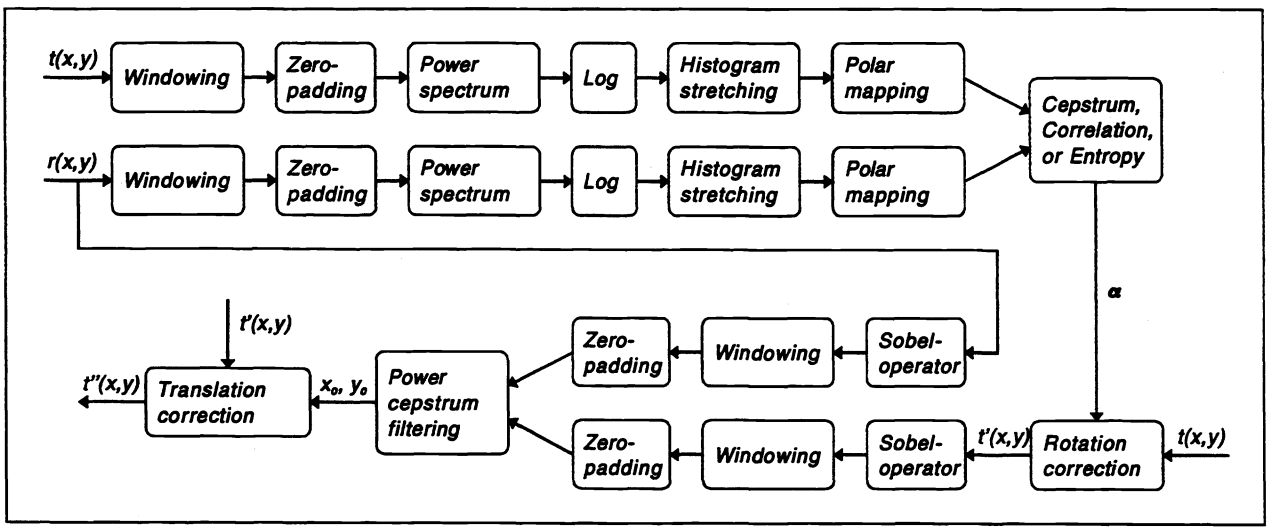

Figure 3: ROTATION–EXTENDED CEPSTRUM TECHNIQUE
After windowing and zero–padding, the Fourier power–spectra of both images to be registered are calculated. Before mapping to polar coordinates, the spectra are histogram optimized. Rotation is detected first using either the classical cepstrum technique, or the correlation, or the entropy based similarity measure. These are the three methods to be compared. After re–rotating one image, the cepstrum technique is applied in a second step also registering translations.

5 TEST IMAGES

Taking into account the influence of real structures in the non–overlapping regions of both radiographs to be registered, we compared the three approaches for the rotation detection step by means of in–vitro acquired digital radiographs of a human jaw (Fig. 4). Therefore, a mechanical device with micrometer screws was constructed fixing the positions of X–ray tube, in–vitro object, and X–ray CCD–sensor. Three image sequences have been generated by equidistantly moving or rotating the sensor perpendicular to the central ray.

- The translation sequence containing 41 frames has been obtained moving the jawbone 40mm perpendicular to the central–ray along the 17.2mm width sensor (Fig. 4 top).
- The combined sequence including 33 images has been acquired rotating the object with a total amount of 180 degrees, while the rotation axis was not in the center of the sensor. Therefore, this sequence contains not only rotations, but also translations (Fig. 4 middle).

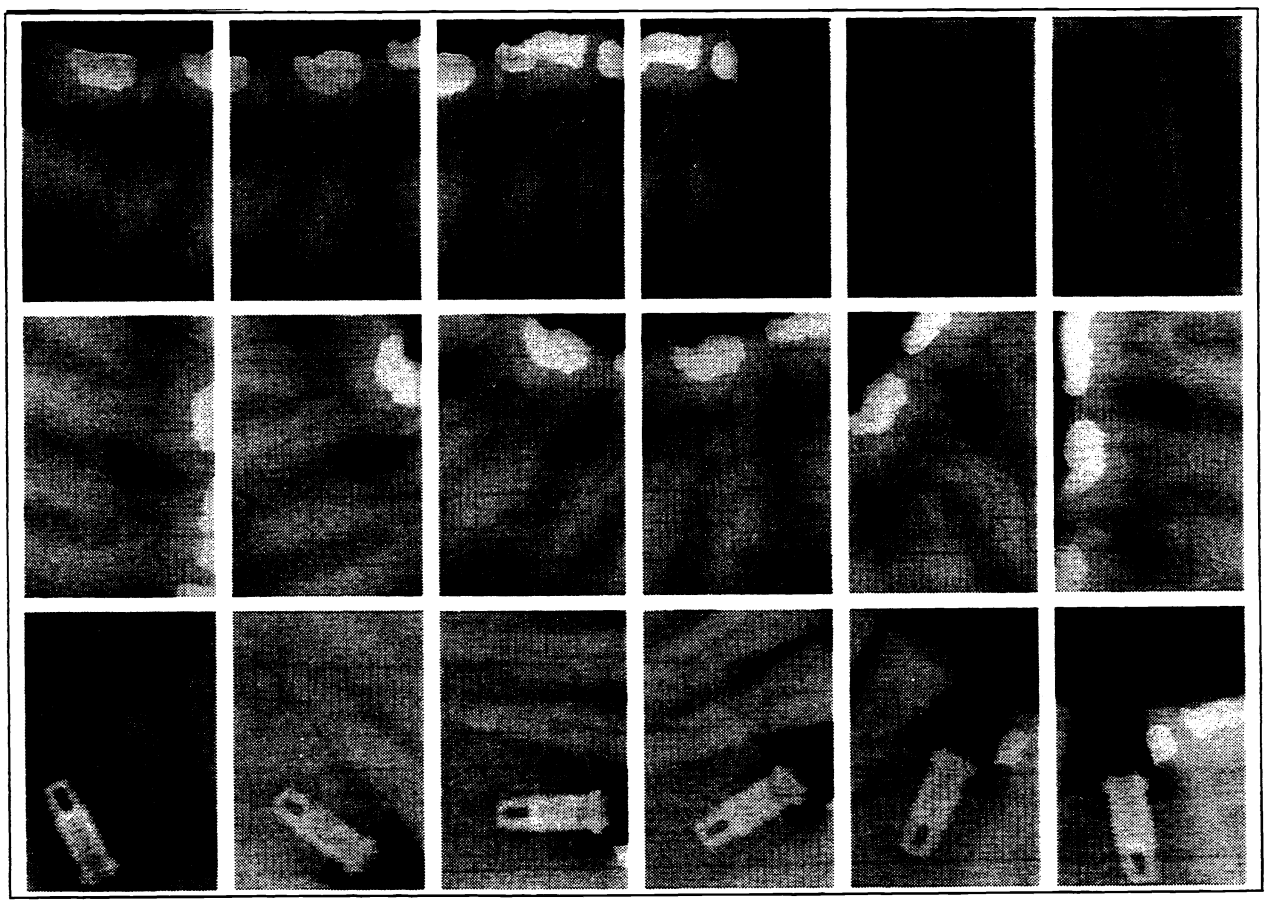

Figure 4: TEST IMAGE SEQUENCES
The three lines show single frames equidistantly captured from the three in–vitro acquired test sequences: top: pure translation, middle: translation and rotation, and bottom: translation, rotation, and intensity variation.

- The third sequence has been produced in a similar way. Additionally, the X ray's dose was modified during the acquisition of the sequence. Therefore, the images differ in intensity and noise. The captured section of the dry mandible includes front teeth, premolars, and a dental implant produced by Branemark (Fig. 4 bottom).

Combinig the sequence's single frames in pairs of twos, altogether 855 different sets of X rays with a priori known relative movement where registered applying all three techniques.

6 RESULTS AND DISCUSSION

Our extensive simulations proved the rotation detection step by means of the cross–correlation or the entropy of the one–dimensional histogram of the difference image to be superior to the one based on the cepstrum filter (Tab. 1). This is because Fourier power–spectra instead of real images are to be adjusted. Since correlation and entropy yield similar results, the entropy method is preferable due to its numerical efficiency. While the correlation has to be computed in a two–dimensional image plane, the entropy is calculated on an one–dimensional histogram function.

Sequence	Displacement	Image pairs	Rotation detection performing					
			Cepstrum		Correlation		Entropy	
		No.	No.	%	No.	%	No.	%
Translation	0.00%	41	41	100	41	100	41	100
	5.81%	40	40	100	40	100	40	100
	11.63%	39	39	100	39	100	39	100
	17.44%	38	36	95	38	100	38	100
	23.26%	37	34	92	34	92	34	92
	→ 29.07%	36	26	72	29	80	30	83
	34.88%	35	20	57	21	60	21	60
	40.70%	34	11	32	15	44	17	50
	46.51%	33	6	18	5	15	7	21
Translation and rotation	0.00°	33	33	100	33	100	33	100
	5.45°	32	29	88	32	100	32	100
	10.90°	31	18	58	31	100	31	100
	→ 16.35°	30	8	27	28	93	29	97
	21.80°	29	6	21	21	72	23	79
	27.25°	28	5	19	19	68	19	68
	32.70°	27	4	15	11	41	12	44
	38.15°	26	5	19	9	34	11	42
	43.60°	25	3	12	6	24	7	28
Translation and rotation and intensity variation	0.00°	33	33	100	33	100	33	100
	5.45°	32	18	56	28	88	30	94
	10.90°	31	13	42	27	87	28	90
	→ 16.35°	30	9	30	22	73	24	80
	21.80°	29	7	24	16	55	19	66
	27.25°	28	2	7	9	32	13	46
	32.70°	27	4	15	11	40	13	48
	38.15°	26	1	4	4	18	9	34
	43.60°	25	0	0	4	16	6	24
Sum		855	451	52.75	606	70.88	639	74.74

Table 1: RESULTS
The table on the left shows the results evaluating 855 pairs of dental radiographs with a priori known displacement. The three horizontal blocks refer to the three captured X–ray sequences (Fig. 4). The second column denotes the relative displacement of the two radiograps being registered. For the rotated sequences, the angle α of rotational movement is given. The third column denotes the overall number of image pairs evaluated with this movement. The block on the right shows the numbers and percentages of correct registrations using the different methods to detect the rotational movement. The columns: Cepstrum, Correlation, and Entropy refer to equations (17), (19), and (21), respectively. The extensive simulations prove the rotation detection by means of cross–correlation or entropy to be superior to the one based on the cepstrum. This can be deducted from the lines marked with an arrow (→).

The union of the logarithmic polar mapped power–spectra with the entropy–measure is precisely reducing rotations. Subsequently, translations are corrected using common cepstral techniques. This technique allows reliable (probabililty > 80%) registration of pictures overlapping more than 70 percent with rotational components less than 15 degrees, regardless of noise or intensity variations occuring in clinical radiographs.

7 CONCLUSION

The common cepstrum technique was restricted so far to the detection of pure translational shifts. Combining the entropy analysis with the Fourier–Mellin RST–invariant image descriptor, cepstrum is now extended to rotations as well. The proposed method is successfully applied as the initial image processing step for the densitrometric analysis of bone lesions in dental radiographs. This initial registration permits the subtraction of sequential images followed by an automatical segmentation of bone lesions and measurement of lesion areas. In dental radiology, radiographs are taken from the same dental region of the same patient at different points of time. Translational as well as rotational misalignments can be precisely compensated in–vivo with the new method even if other distortions of the projective geometry occur.

The two in–vitro X rays shown in Figure 1 were registrated applying the new technique. After cepstral filtering, the subtraction of both images proves their successful registration (Fig. 5). This shows the rotation–extended cepstrum technique to be the fundamental part of the densitometric analysis of the alveolar bone structures.

8 REFERENCES

1. T. Lehmann, C. Goerke, A. Kaupp, R. Repges, "Cepstrum Analysis Extended to Rotational and Translational Registration," *Proceedings of the Third International Conference on Pattern Recognition and Information Analysis PRIA'95 in Minsk, Belarus,* S. Ablameyko, J. Soldek, Vol. 3, pp. 111–115, Zapol Press, Szczecin, 1995.
2. A. V. Cideciyan, "Registration of Ocular Fundus Images," *IEEE Magazine EMB,* Vol. EMB–14, pp. 52–58, Jan. 1995.

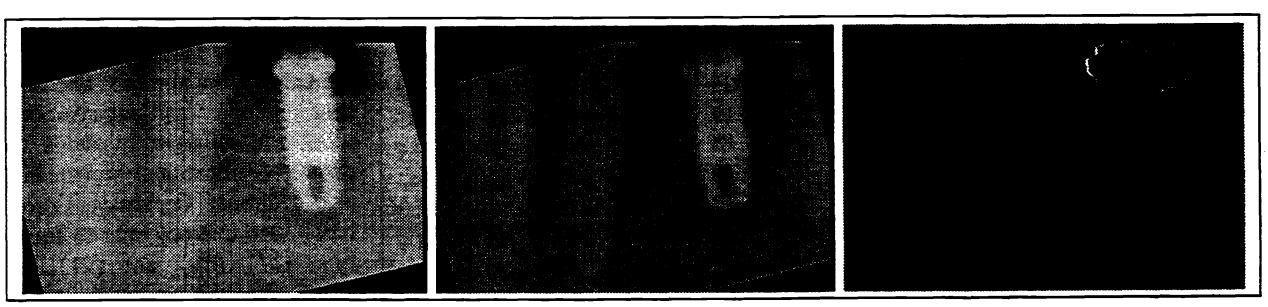

Figure 5: REGISTRATION OF ROTATIONS AND TRANSLATIONS USING THE CEPSTRUM TECHNIQUE
The in–vitro radiograph shown in Figure 1 in the left of the bottom line was adjusted to the reference image (Fig. 1 top left) using the rotation-extended cepstrum technique. After geometrical (left) and contrast (middle) adjustment, the reference image was subtracted from the subsequent image (right). The simulated changes in bone structure are clearly visible as dark spots in the difference image. The black and white borders of the implant are artefacts caused by misalignment.

3. Q. S. Chen, M. Defrise, F. Deconinck, "Symmetric Phase–Only Matched Filtering of Fourier–Mellin Transforms for Image Registration and Recognition," *IEEE Trans. on PAMI,* Vol. PAMI–16, pp. 1156–1168, Dez. 1994.
4. W. K. Pratt, *Digital Image Processing,* John Wiley & Sons, New York, 1978.
5. T. H. Reiss, *Recognizing Planar Objects Using Invariant Image Features,* Springer–Verlag, Berlin, 1993.
6. P. F. van der Stelt, U. E. Ruttimann, R. L. Webber, "Determination of projections for subtraction radiography based on image similarity measurements," *Dentomaxillofacial Radiology,* Vol. 18, pp. 113–117, 1989.
7. S. M. Dunn, P. F. van der Stelt, K. Fenesy, S. Shah, "A comparison of two registration techniques for digital subtraction radiography," *Dentomaxillofacial Radiology,* Vol. 22, pp. 77–80, 1993.
8. A. Venot, J. F. Lebruchec, J. C. Roucayrol, "A new class of similarity measures for robust image registration," *Computer Vision, Graphics, and Image Processing,* Vol. 28, pp. 176–184, 1984.
9. A. Venot, V. Leclerc, "Automated correlation of patient motion and grey value prior to subtraction in digitized angiography," *IEEE Trans. on MI,* Vol. MI–3, pp. 179–186, 1984.
10. D. J. Lee, S. Mitra, T. F. Krile, "Analysis of sequential complex images, using feature extraction and two–dimensional cepstrum techniques," *Journal of the Optical Society of America A,* Vol. JOSA A–6, pp. 863–870, 1989.
11. R. N. Bracewell, *The Fourier Transform and Its Applications,* 2nd Edition, McGraw–Hill, New York, 1986.
12. S. Colombo, J. Lavoine, *Transformations de Laplace et de Mellin. Formulaires. Mode D'Utilisation,* Gauthier–Villars, Paris, 1972.
13. F. Oberhettinger, *Tables of Mellin Transforms,* Springer–Verlag, Berlin, 1974.
14. R. J. Schalkoff, *Digital Image Processing and Computer Vision,* John Wiley & Sons, New York, 1989.
15. H. Haken, *Synergetic Computers and Cognition. A Top–Down Approach to Neural Nets,* Springer–Verlag, Berlin, 1991.
16. T. Lehmann, C. Goerke, W. Schmitt, R. Repges, "Rotations– und Translationsbestimmung durch eine erweiterte Kepstrum–Technik," *Mustererkennung 1995 · Verstehen akustischer und visueller Information,* G. Sagerer, S. Posch, F. Kummert, Reihe Informatik aktuell, pp. 395–402, Springer–Verlag, Berlin, 1995.
17. B. P. Bogert, M. J. R. Healy, J. W. Tukey, "The Quefrency Alanysis of Time Series for Echoes: Cepstrum, Pseudo–Autovariance, Cross–Cepstrum and Saphe Cracking," *Proceedings of the Symposium of Time Series Analysis,* pp. 209–242, 1963.
18. D. G. Childers, D. P. Skinner, R. C. Kemerait, "The Cepstrum: A Guide to Processing," *Procs. of the IEEE,* Vol. 65, pp. 1428–1443, Okt. 1977.
19. A. V. Oppenheim, R. W. Schafer, *Digital Signal Processing,* Prentice–Hall, Englewood Cliffs, 1975.
20. A. Wenzel, "Effect of manual compared with reference point superimposition on image quality in digital subtraction radiography," *Dentomaxillofacial Radiology,* Vol. 18, pp. 145–150, 1989.
21. J. N. Kapur, P. K. Sahoo, A. K. C. Wong, "A New Method for Gray–Level Picture Thresholding Using the Entropy of the Histogram," Computer Vision, Graphics, and Image Processing, Vol. 29, pp. 273–285, 1985.
22. T. Lehmann, W. Schmitt, R. Repges, A. Sovakar, "Mathematical Quality Standards for the Digital Free–hand Subtraction Radiography," *Dentomaxillofacial Radiology,* Vol. 24, p. 98, 1995.
23. F. J. Harris, "On the Use of Windows for Harmonic Analysis with the Discrete Fourier–Transform," *Proceedings of the IEEE,* Vol. 66, pp. 51–83, 1978.
24. M. C. Steckner, D. J. Drost, "Fast Cepstrum Analysis Using the Hartley Transform," *IEEE Trans. on ASSP,* Vol ASSP–37, pp. 1300–1302, 1989.
25. R. N. Bracewell, "The Discrete Hartley Transform," *Journal of the Optical Society of America A,* Vol. JOSA 73, pp. 1832-1835, 1983.
26. R. N. Bracewell, *The Hartley Transform,* Oxford University Press, New York, 1986.
27. R. V. L. Hartley, "A more symmetrical Fourier analysis applied to transmission problems," *Proc. IRE,* Vol. 30, pp. 144–150, 1942.
28. A. B. Watson, A. Poirson, "Separable two–dimensional discrete Hartley–transform," *Journal of the Optical Society of America A,* Vol. JOSA A–3, pp. 2001–2004, 1986.
29. R. N. Bracewell, "The Fast Hartley Transform," *Proceedings of the IEEE,* Vol. 72, pp. 1010–1018, 1984.
30. P. W. Besslich, T. Lu, *Diskrete Orthogonaltransformationen,* Springer–Verlag, Berlin, 1990.